Nonlinear Dyn (2013) 72:517–537
DOI 10.1007/s11071-012-0731-5

ORIGINAL PAPER

Positive position feedback (PPF) controller for suppression of nonlinear system vibration

W.A. El-Ganaini · N.A. Saeed · M. Eissa

Received: 4 October 2012 / Accepted: 19 December 2012 / Published online: 16 January 2013

Abstract In this paper, a study for positive position feedback controller is presented that is used to suppress the vibration amplitude of a nonlinear dynamic model at primary resonance and the presence of 1:1 internal resonance. We obtained an approximate solution by applying the multiple scales method. Then we conducted bifurcation analyses for open and closed loop systems. The stability of the system is investigated by applying the frequency-response equations. The effects of the different controller parameters on the behavior of the main system have been studied. Optimum working conditions of the system were extracted to be used in the design of such systems. Finally, numerical simulations are performed to demonstrate and validate the control law. We found that all predictions from analytical solutions are in good agreement with the numerical simulation. A comparison with the available published work is included at the end of the work.

Keywords Vibration control · Positive position feedback · Stability · Primary resonance

Nomenclature

$u, \dot{u}, \ddot{u}$	Displacement, velocity and acceleration of main system, respectively
$v, \dot{v}, \ddot{v}$	Displacement, velocity and acceleration of controller, respectively
μ_1, μ_2	Linear damping parameters of main system and controller, respectively
ω_1, ω_2	Linear natural frequencies of main system and controller, respectively
α_1, α_2	Cubic nonlinearity parameters of main system and controller, respectively
δ	Main system nonlinear parameter
f	External excitation force amplitude
Ω	External excitation frequency
F_c	Control signal
F_f	Feedback signal
γ	Control signal gain
λ	Feedback signal gain
ε	Small perturbation parameter

1 Introduction

Vibration, occurring in most machines, vehicles, structures, building and dynamic systems is undesirable, not only because of the resulting unpleasant motions, the dynamic stresses which may lead to fatigue and failure of the structure or machine, the energy losses and reduction in performance which accompany vibrations, but also because of the produced noise. Noise is an undesired phenomenon, and since sound is produced by some source of motion or vibration causing

W.A. El-Ganaini · N.A. Saeed (✉) · M. Eissa
Department of Physics and Engineering Mathematics, Faculty of Electronic Engineering, Menoufia University, Menouf 32952, Egypt
e-mail: eng_saeed_2003@yahoo.com

pressure changes which propagate through the air or other transmitting medium, vibration control is of vital importance to sound attenuation. Vibration analysis of machines and structures is often a necessary prerequisite for controlling vibration and noise. The theory and techniques of vibration suppression have been extensively studied for many years. Various types of controller are developed so as to channel the excess energy from excitation to the slave system in order that vibration in the primary system can be suppressed. The positive position feedback (PPF) controller used extensively for vibration reduction for many linear and nonlinear dynamical systems, which show their feasibility and efficiency in practice. Warminski et al. [1] studied active suppression of nonlinear composite beam vibrations by selected control algorithms. Shan et al. [2] studied slewing and vibration control of a single-link flexible manipulator by positive position feedback controller. Wang et al. [3] presented theoretical and experimental study of active vibration control of a flexible cantilever beam using piezoelectric actuators. Creasy et al. [4] discussed adaptive positive position feedback controller for actively absorbing energy in acoustic cavities. Ahamed et al. [5] presented dynamic compensation for control of a rotary wing unmanned aerial vehicle (UAV) using positive position feedback controller. Baz et al. [6] studied optimal vibration control with modal positive position feedback controller. Baz et al. [7] presented a study for daptive control of flexible structures using modal positive position feedback controller. In Refs. [8–10] the authors presented a study for single mode control of a cantilever beam under primary and principal parametric excitation. Nonlinear vibrations of primary and parametrically excited cantilever beams subjected to nonlinear delayed feedback control are investigated in Refs. [11, 12]. Eissa et al. [13–21] studied the vibration reduction for various systems using different passive and active control techniques.

In this paper, we applied positive position feedback active controller to suppress the vibration of a nonlinear system when subjected to external primary resonance excitation. The multiple scale perturbation method is applied to obtain a first-order approximate solution. The equilibrium curves for various controller parameters are plotted. The stability of the steady state solution is investigated using frequency-response equations. The approximate solution was numerically verified. We found that all predictions from analytical solutions are in good agreement with the numerical simulation. Finally, a comparison with the available published work is included by the end of the work.

2 System model

The nonlinear ordinary differential equation that describes the dynamical behavior of the considered system is given in Ref. [1] as

$$\ddot{u} + 2\mu_1\omega_1\dot{u} + \omega_1^2 u + \alpha_1 u^3 - \delta\left(u\dot{u}^2 + u^2\ddot{u}\right) = f\cos(\Omega t) + \gamma F_c(t) \tag{1}$$

We introduce a second order nonlinear controller, which is coupled to the main system through a control law. Then, the equation governing the dynamics of the controller (PPF) is suggested as

$$\ddot{v} + 2\mu_2\omega_2\dot{v} + \omega_2^2 v + \alpha_2 v^3 = \lambda F_f(t) \tag{2}$$

We choose the control signal $F_c = v$, and the feedback signal $F_f = u$, so the closed loop system equations are

$$\ddot{u} + 2\mu_1\omega_1\dot{u} + \omega_1^2 u + \alpha_1 u^3 - \delta\left(u\dot{u}^2 + u^2\ddot{u}\right) = f\cos(\Omega t) + \gamma v \tag{3}$$

$$\ddot{v} + 2\mu_2\omega_2\dot{v} + \omega_2^2 v + \alpha_2 v^3 = \lambda u \tag{4}$$

3 Perturbation analysis

Applying the multiple scales method [22], we obtain first-order approximate solutions for (3) and (4) by seeking the solutions in the forms

$$u(T_0, T_1, \varepsilon) = \varepsilon u_1(T_0, T_1) + \varepsilon^2 u_2(T_0, T_1) \tag{5}$$

$$v(T_0, T_1, \varepsilon) = \varepsilon v_1(T_0, T_1) + \varepsilon^2 v_2(T_0, T_1) \tag{6}$$

where ε is a small dimensionless book-keeping perturbation parameter and $0 < \varepsilon \ll 1$, $T_0 = t$ and $T_1 = \varepsilon t$ are the fast and slow time scales, respectively. In terms of T_0 and T_1, the time derivatives are transformed into

$$\frac{d}{dt} = D_0 + \varepsilon D_1, \qquad \frac{d^2}{dt^2} = D_0^2 + 2\varepsilon D_0 D_1$$

$$\text{where } D_j = \frac{\partial}{\partial T_j},\ j = 0, 1 \tag{7}$$

To make damping, nonlinearities, primary resonance excitation force, feedback gain and control signal gain

appear in the same perturbation equations, we scale the equations parameters as

$$\mu_n = \varepsilon\hat{\mu}_n, \qquad \alpha_n = \varepsilon^{-1}\hat{\alpha}_n, \qquad \delta = \varepsilon^{-1}\hat{\delta},$$
$$\lambda = \varepsilon\hat{\lambda}, \qquad \gamma = \varepsilon\hat{\gamma} \quad \text{and} \quad f = \varepsilon^2\hat{f}, \quad n = 1, 2 \tag{8}$$

Substituting (5) to (8) into (3) and (4), and equating coefficients of like powers of ε, we obtain the following set of ordinary differential equations:

O(ε):

$$\left(D_0^2 + \omega_1^2\right)u_1 = 0 \tag{9}$$

$$\left(D_0^2 + \omega_2^2\right)v_1 = 0 \tag{10}$$

O(ε^2):

$$\begin{aligned}\left(D_0^2 + \omega_1^2\right)u_2 = {} & -\hat{\alpha}_1 u_1^3 + \hat{\gamma} v_1 - 2\hat{\mu}_1\omega_1 D_0 u_1 \\ & - 2D_1 D_0 u_1 + \hat{\delta} u_1^2 D_0^2 u_1 \\ & + \hat{\delta} u_1 (D_0 u_1)^2 \\ & + \frac{\hat{f}}{2}\left(e^{i\Omega T_0} + e^{-i\Omega T_0}\right)\end{aligned} \tag{11}$$

$$\begin{aligned}\left(D_0^2 + \omega_2^2\right)v_2 = {} & \hat{\lambda} u_1 - \hat{\alpha}_2 v_1^3 - 2D_1 D_0 v_1 \\ & - 2\hat{\mu}_2\omega_2 D_0 v_1\end{aligned} \tag{12}$$

The general solution of (9) and (10) can be expressed in the forms:

$$u_1(T_0, T_1) = A(T_1)e^{i\omega_1 T_0} + cc \tag{13}$$

$$v_1(T_0, T_1) = B(T_1)e^{i\omega_2 T_0} + cc \tag{14}$$

where cc stands for the complex conjugate of the preceding terms. The quantities $A(T_1)$ and $B(T_1)$ are unknown function in T_1 at this stage of the analysis. They will be determined by eliminating the secular and small-divisor terms at the next approximation order.

Substituting (13) and (14) into (11) and (12), we get

$$\begin{aligned}\left(D_0^2 + \omega_1^2\right)u_2 = {} & \hat{\gamma} B e^{i\omega_2 T_0} - \left[\hat{\alpha}_1 A^3 + 2\hat{\delta}\omega_1^2 A^3\right]e^{3i\omega_1 T_0} \\ & + \left[-3\hat{\alpha}_1 A^2\overline{A} - 2\hat{\delta}\omega_1^2 A^2\overline{A}\right. \\ & \left. - 2i\hat{\mu}_1\omega_1^2 A - 2i\omega_1 D_1 A\right]e^{i\omega_1 T_0} \\ & + \frac{\hat{f}}{2}e^{i\Omega T_0} + cc\end{aligned} \tag{15}$$

$$\begin{aligned}\left(D_0^2 + \omega_2^2\right)v_2 = {} & \hat{\lambda} A e^{i\omega_1 T_0} - \hat{\alpha}_2 B^3 e^{3i\omega_2 T_0} \\ & + \left[-2i\omega_2 D_1 B - 3\hat{\alpha}_2 B^2\overline{B}\right. \\ & \left. - 2i\hat{\mu}_2\omega_2^2 B\right]e^{i\omega_2 T_0} + cc\end{aligned} \tag{16}$$

where the over bar denotes the complex conjugate functions. The particular solutions of (15) and (16) take the forms

$$u_2 = \theta_1 e^{i\omega_2 T_0} + \theta_2 e^{3i\omega_1 T_0} + \theta_3 e^{i\Omega T_0} + cc \tag{17}$$

$$v_2 = \theta_4 e^{i\omega_1 T_0} + \theta_5 e^{3i\omega_2 T_0} + cc \tag{18}$$

where

$$\theta_1 = \frac{\hat{\gamma} B}{\omega_1^2 - \omega_2^2}, \qquad \theta_2 = \frac{\hat{\alpha}_1 A^3 + 2\hat{\delta}\omega_1^2 A^3}{8\omega_1^2},$$
$$\theta_3 = \frac{\hat{f}}{2(\omega_1^2 - \Omega^2)}, \qquad \theta_4 = \frac{\hat{\lambda} A}{\omega_2^2 - \omega_1^2}, \quad \text{and}$$
$$\theta_5 = \frac{\hat{\alpha}_2 B^3}{8\omega_2^2}.$$

The deduced resonance conditions in this approximation order are:

(i) Primary resonance: $\Omega = \omega_1$
(ii) Internal resonance: $\omega_1 = \omega_2$
(iii) Simultaneous resonance: $\Omega = \omega_1$ and $\omega_1 = \omega_2$

In this work, the case of the simultaneous resonances ($\Omega = \omega_1, \omega_1 = \omega_2$) is considered. So, the closeness of the simultaneous resonances can be described quantitatively by introducing the detuning parameters σ_1 and σ_2 according to:

$$\begin{aligned}\Omega &= \omega_1 + \sigma_1 = \omega_1 + \varepsilon\hat{\sigma}_1, \\ \omega_2 &= \omega_1 + \sigma_2 = \omega_1 + \varepsilon\hat{\sigma}_2\end{aligned} \tag{19}$$

Inserting (19) into the secular and small-divisor terms in (15) and (16), one finds the solvability conditions:

$$\begin{aligned}&\left[-3\hat{\alpha}_1 A^2\overline{A} - 2\hat{\delta}\omega_1^2 A^2\overline{A} - 2i\hat{\mu}_1\omega_1^2 A - 2i\omega_1 D_1 A\right] \\ &\quad \times e^{i\omega_1 T_0} + \hat{\gamma} B e^{i\hat{\sigma}_2 T_1} e^{i\omega_1 T_0} \\ &\quad + \frac{\hat{f}}{2}e^{i\hat{\sigma}_1 T_1} e^{i\omega_1 T_0} = 0\end{aligned} \tag{20}$$

$$\begin{aligned}&\left[-2i\omega_2 D_1 B - 3\hat{\alpha}_2 B^2\overline{B} - 2i\hat{\mu}_2\omega_2^2 B\right]e^{i\omega_2 T_0} \\ &\quad + \hat{\lambda} A e^{-i\hat{\sigma}_2 T_1} e^{i\omega_2 T_0} = 0\end{aligned} \tag{21}$$

Dividing (20) by $e^{i\omega_1 T_0}$ and (21) by $e^{i\omega_2 T_0}$, we get

$$-3\hat{\alpha}_1 A^2\overline{A} - 2\hat{\delta}\omega_1^2 A^2\overline{A} - 2i\hat{\mu}_1\omega_1^2 A - 2i\omega_1 D_1 A + \hat{\gamma} B e^{i\hat{\sigma}_2 T_1} + \frac{\hat{f}}{2} e^{i\hat{\sigma}_1 T_1} = 0 \tag{22}$$

$$-2i\omega_2 D_1 B - 3\hat{\alpha}_2 B^2\overline{B} - 2i\hat{\mu}_2\omega_2^2 B + \hat{\lambda} A e^{-i\hat{\sigma}_2 T_1} = 0 \tag{23}$$

To analyze the solution of (22) and (23), we put

$$A(T_1) = (\hat{a}_1/2)e^{i\beta_1} \quad \Rightarrow \quad D_1 A(T_1) = (\hat{a}_1'/2)e^{i\beta_1} + i(\hat{a}_1\beta_1'/2)e^{i\beta_1}, \quad a_1 = \varepsilon\hat{a}_1 \tag{24}$$

$$B(T_1) = (\hat{a}_2/2)e^{i\beta_2} \quad \Rightarrow \quad D_1 B(T_1) = (\hat{a}_2'/2)e^{i\beta_2} + i(\hat{a}_2\beta_2'/2)e^{i\beta_2}, \quad a_2 = \varepsilon\hat{a}_2 \tag{25}$$

where $()' = D_1()$, a_1 and a_2 are the steady-state amplitudes of the main system and controller, respectively, and β_1, β_2 are the phases of the motion. Inserting (24) and (25) into (22) and (23), we get the following amplitude-phase modulating equations:

$$\dot{a}_1 = -(\mu_1\omega_1)a_1 + \left(\frac{\gamma}{2\omega_1}\right)a_2\sin(\varphi_2) + \left(\frac{f}{2\omega_1}\right)\sin(\varphi_1) \tag{26}$$

$$a_1\dot{\beta}_1 = \left(\frac{3\alpha_1}{8\omega_1}\right)a_1^3 + \left(\frac{\delta\omega_1}{4}\right)a_1^3 - \left(\frac{\gamma}{2\omega_1}\right)a_2\cos(\varphi_2) - \left(\frac{f}{2\omega_1}\right)\cos(\varphi_1) \tag{27}$$

$$\dot{a}_2 = -(\mu_2\omega_2)a_2 - \left(\frac{\lambda}{2\omega_2}\right)a_1\sin(\varphi_2) \tag{28}$$

$$a_2\dot{\beta}_2 = \left(\frac{3\alpha_2}{8\omega_2}\right)a_2^3 - \left(\frac{\lambda}{2\omega_2}\right)a_1\cos(\varphi_2) \tag{29}$$

where

$$\dot{()} = d()/dt, \qquad \varphi_1 = \hat{\sigma}_1 T_1 - \beta_1 = \sigma_1 t - \beta_1, \qquad \varphi_2 = \hat{\sigma}_2 T_1 + \beta_2 - \beta_1 = \sigma_2 t + \beta_2 - \beta_1 \tag{30}$$

To eliminate $\dot{\beta}_1$ and $\dot{\beta}_2$ from equations (27) and (29), by differentiating (30) with respect to t, we have

$$\dot{\beta}_1 = \sigma_1 - \dot{\varphi}_1, \qquad \dot{\beta}_2 = (\dot{\varphi}_2 - \dot{\varphi}_1 + \sigma_1 - \sigma_2) \tag{31}$$

Substituting (31) into (27) and (29), we obtain

$$\dot{\varphi}_1 = \sigma_1 - \frac{3}{8\omega_1}\alpha_1 a_1^2 - \frac{1}{4}\delta\omega_1 a_1^2 + \frac{1}{2a_1\omega_1}\gamma a_2\cos(\varphi_2) + \frac{1}{2a_1\omega_1} f\cos(\varphi_1) \tag{32}$$

$$\dot{\varphi}_2 = \sigma_2 - \left[\frac{1}{4}\delta\omega_1 + \frac{3}{8\omega_1}\alpha_1\right]a_1^2 + \frac{3}{8\omega_2}\alpha_2 a_2^2 + \left[\frac{1}{2a_1\omega_1}\gamma a_2 - \frac{1}{2\omega_2 a_2}\lambda a_1\right]\cos(\varphi_2) + \frac{1}{2a_1\omega_1} f\cos(\varphi_1) \tag{33}$$

From (26), (28), (32), and (33), the autonomous amplitude-phase modulating equations are

$$\dot{a}_1 = -\mu_1\omega_1 a_1 + \frac{1}{2\omega_1}\gamma a_2\sin(\varphi_2) + \frac{1}{2\omega_1} f\sin(\varphi_1) \tag{34a}$$

$$\dot{\varphi}_1 = \sigma_1 - \frac{3}{8\omega_1}\alpha_1 a_1^2 - \frac{1}{4}\delta\omega_1 a_1^2 + \frac{1}{2a_1\omega_1}\gamma a_2\cos(\varphi_2) + \frac{1}{2a_1\omega_1} f\cos(\varphi_1) \tag{34b}$$

$$\dot{a}_2 = -\mu_2\omega_2 a_2 - \frac{1}{2\omega_2}\lambda a_1\sin(\varphi_2) \tag{34c}$$

$$\dot{\varphi}_2 = \sigma_2 - \left[\frac{1}{4}\delta\omega_1 + \frac{3}{8\omega_1}\alpha_1\right]a_1^2 + \frac{3}{8\omega_2}\alpha_2 a_2^2 + \left[\frac{1}{2a_1\omega_1}\gamma a_2 - \frac{1}{2\omega_2 a_2}\lambda a_1\right]\cos(\varphi_2) + \frac{1}{2a_1\omega_1} f\cos(\varphi_1) \tag{34d}$$

The performance of the control law will be evaluated by calculating the equilibrium solutions of (34a)–(34d), and examining their stability as a function in the parameters $\sigma_1, \sigma_2, \mu_2, \alpha_2, \omega_2, \gamma, \lambda$, and f.

4 Equilibrium solution

At steady-state motion we have

$$\dot{a}_1 = \dot{a}_2 = \dot{\varphi}_1 = \dot{\varphi}_2 = 0 \tag{35}$$

This corresponds to the equilibrium points of (34a)–(34d). Substituting (35) into (31), we get

$$\dot{\beta}_1 = \sigma_1, \qquad \dot{\beta}_2 = \sigma_1 - \sigma_2 \tag{36}$$

Substituting (35) and (36) into (26) to (29), we get

$$\mu_1\omega_1 a_1 = \frac{1}{2\omega_1}\gamma a_2 \sin(\varphi_2) + \frac{1}{2\omega_1} f \sin(\varphi_1) \tag{37}$$

$$\sigma_1 = \frac{3}{8\omega_1}\alpha_1 a_1^2 + \frac{1}{4}\delta\omega_1 a_1^2 - \frac{1}{2a_1\omega_1}\gamma a_2 \cos(\varphi_2) - \frac{1}{2a_1\omega_1} f \cos(\varphi_1) \tag{38}$$

$$\mu_2\omega_2^2 a_2 = -\frac{1}{2}\lambda a_1 \sin(\varphi_2) \tag{39}$$

$$\omega_2(\sigma_1 - \sigma_2)a_2 - \frac{3}{8}\alpha_2 a_2^3 = -\frac{1}{2}\lambda a_1 \cos(\varphi_2) \tag{40}$$

Squaring and adding (39) and (40), we get

$$\mu_2^2\omega_2^4 a_2^2 + \left[\omega_2(\sigma_1 - \sigma_2)a_2 - \frac{3}{8}\alpha_2 a_2^3\right]^2 = \frac{1}{4}\lambda^2 a_1^2 \tag{41}$$

From (39) and (40), we have

$$\sin(\varphi_2) = -\frac{2\mu_2\omega_2^2 a_2}{\lambda a_1} \tag{42}$$

$$\cos(\varphi_2) = -\frac{1}{\lambda a_1}\left(2\omega_2(\sigma_1 - \sigma_2)a_2 - \frac{3}{4}\alpha_2 a_2^3\right) \tag{43}$$

Inserting (42) and (43) into (37) and (38), we get

$$\mu_1\omega_1 a_1 + \frac{1}{\omega_1\lambda a_1}\gamma\mu_2\omega_2^2 a_2^2 = \frac{1}{2\omega_1} f \sin(\varphi_1) \tag{44}$$

$$\frac{3}{8\omega_1}\alpha_1 a_1^3 + \frac{1}{4}\delta\omega_1 a_1^3 + \frac{\gamma}{\lambda\omega_1 a_1} \times \left(\omega_2(\sigma_1 - \sigma_2)a_2^2 - \frac{3}{8}\alpha_2 a_2^4\right) - \sigma_1 a_1 = \frac{1}{2\omega_1} f \cos(\varphi_1) \tag{45}$$

Squaring and adding equations (44) and (45), we get

$$\left[\frac{3}{8\omega_1}\alpha_1 a_1^3 + \frac{1}{4}\delta\omega_1 a_1^3 + \frac{\gamma}{\lambda\omega_1 a_1}\left(\omega_2(\sigma_1 - \sigma_2)a_2^2 - \frac{3}{8}\alpha_2 a_2^4\right) - \sigma_1 a_1\right]^2 + \left[\mu_1\omega_1 a_1 + \frac{1}{\omega_1\lambda a_1}\gamma\mu_2\omega_2^2 a_2^2\right]^2 = \frac{1}{4\omega_1^2} f^2 \tag{46}$$

Equations (41) and (46) are the frequency-response equations that used to describes the system steady-state solutions behavior for the practical case i.e. ($a_1 \neq 0, a_2 \neq 0$).

5 Stability analysis

The stability of the equilibrium solution was determined by examining the eigenvalues of the Jacobian matrix of the right-hand side of (34a)–(34d). If the real part of each eigenvalue is negative, the corresponding equilibrium solution is asymptotically stable. If the real part of any eigenvalues is positive, the corresponding equilibrium solution is unstable. To derive the stability criteria, we need to examine the behavior of small deviations from the steady-state solutions $a_{10}, a_{20}, \varphi_{10}$, and φ_{20}. Thus, we assume that

$$\left.\begin{aligned} &a_1 = a_{11} + a_{10}, \qquad a_2 = a_{21} + a_{20}, \\ &\varphi_1 = \varphi_{11} + \varphi_{10}, \qquad \varphi_2 = \varphi_{21} + \varphi_{20} \\ &\dot{a}_1 = \dot{a}_{11}, \qquad \dot{a}_2 = \dot{a}_{21}, \qquad \dot{\varphi}_1 = \dot{\varphi}_{11}, \\ &\dot{\varphi}_2 = \dot{\varphi}_{21} \end{aligned}\right\} \tag{47}$$

where $a_{10}, a_{20}, \varphi_{10}$ and φ_{20} satisfy (41) and (46) and $a_{11}, a_{21}, \varphi_{11}, \varphi_{21}$ are perturbations which are assumed to be small compared to $a_{10}, a_{20}, \varphi_{10}$ and φ_{20}. Substituting (47) into (34a)–(34d), expanding for small $a_{11}, a_{21}, \varphi_{11}$ and φ_{21}, and keeping linear terms in $a_{11}, a_{21}, \varphi_{11}$ and φ_{21}, we get

$$\dot{a}_{11} = r_{11}a_{11} + r_{12}\varphi_{11} + r_{13}a_{21} + r_{14}\varphi_{21} \tag{48}$$

$$\dot{\varphi}_{11} = r_{21}a_{11} + r_{22}\varphi_{11} + r_{23}a_{21} + r_{24}\varphi_{21} \tag{49}$$

$$\dot{a}_{21} = r_{31}a_{11} + r_{32}\varphi_{11} + r_{33}a_{21} + r_{34}\varphi_{21} \tag{50}$$

$$\dot{\varphi}_{21} = r_{41}a_{11} + r_{42}\varphi_{11} + r_{43}a_{21} + r_{44}\varphi_{21} \tag{51}$$

where r_{ij}, $i = 1, 2, 3, 4$ and $j = 1, 2, 3, 4$ are given in the Appendix.

Equations (48) to (51) can be represented in the following matrix form:

$$\begin{bmatrix}\dot{a}_{11} & \dot{\varphi}_{11} & \dot{a}_{21} & \dot{\varphi}_{21}\end{bmatrix}^T = [J]\begin{bmatrix}a_{11} & \varphi_{11} & a_{21} & \varphi_{21}\end{bmatrix}^T \tag{52}$$

where

$$[J] = \begin{bmatrix} r_{11} & r_{12} & r_{13} & r_{14} \\ r_{21} & r_{22} & r_{23} & r_{24} \\ r_{31} & r_{32} & r_{33} & r_{34} \\ r_{41} & r_{42} & r_{43} & r_{44} \end{bmatrix},$$

is the Jacobian matrix.

Thus, the stability of the steady-state solutions depends on the eigenvalues of the Jacobian matrix. One can obtain the following eigenvalue equation:

$$\begin{vmatrix} r_{11}-\lambda & r_{12} & r_{13} & r_{14} \\ r_{21} & r_{22}-\lambda & r_{23} & r_{24} \\ r_{31} & r_{32} & r_{33}-\lambda & r_{34} \\ r_{41} & r_{42} & r_{43} & r_{44}-\lambda \end{vmatrix} = 0 \qquad (53)$$

Expanding this determinant, yields

$$\lambda^4 + \eta_1\lambda^3 + \eta_2\lambda^2 + \eta_3\lambda + \eta_4 = 0 \qquad (54)$$

where λ denotes eigenvalues of the matrix $[J]$, and η_1, η_2, η_3 and η_4 are coefficients of (54). Routh–Hurwitz criterion is used to establish the stability of the equilibrium solutions. Accordingly, the necessary and sufficient conditions for stable system are:

$$\begin{aligned} &\eta_1 > 0, \qquad \eta_1\eta_2 - \eta_3 > 0, \\ &\eta_3(\eta_1\eta_2 - \eta_3) - \eta_1^2\eta_4 > 0, \qquad \eta_4 > 0. \end{aligned} \qquad (55)$$

6 Results and discussions

In this section, the steady-state response of the main system and the controller are investigated extensively for the different controller parameters under primary resonance excitation at the presence of 1:1 internal resonance. Results are presented in graphical forms as steady-state amplitudes versus the detuning parameters and the excitation force f for both the main system and the controller. Figures 1 to 14 are plotted by adopting the following values of the system parameters $\mu_1 = 0.01, \mu_2 = 0.001, \omega_1 = \omega_2 = 3.0, \alpha_1 = 14.5, \alpha_2 = 0.0, \delta = 1.0, \lambda = 2.0, \gamma = 2.0, \sigma_2 = 0.0$, and $f = 0.05$, unless otherwise specified. Solid lines correspond to stable solutions, while dashed ones correspond to unstable solutions.

Figure 1 shows the frequency-response curves for the open loop case (controller not in action) for various levels of the excitation amplitude f. The amplitude of the response depends on the detuning parameter σ_1 and the amplitude of excitation f. It is clear from Fig. 1 that, when the amplitude of excitation f is increased, the frequency response curves of the main system is bent to the right that leading to the hardening effect and jump phenomenon occurrence. As the forcing amplitude increases, the nonlinearity will dominate the main system response.

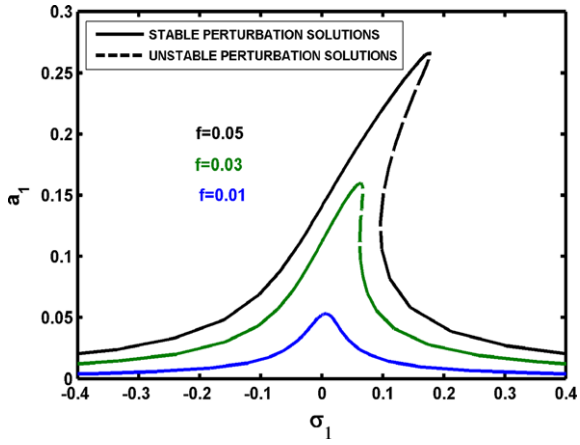

Fig. 1 Uncontrolled system frequency-response curves

Figure 2 shows the controlled system frequency-response curves, where Fig. 2a shows the main system frequency-response curves and Fig. 2b shows the controller frequency-response curves. It is clear that the minimum steady-state amplitude of the main system a_1 occurs when $\sigma_1 = 0.0$ which confirms that the controller is able to suppress the primary resonance vibration effectively. Also, the jumping phenomena associated with each mode are indicated by arrows, where, as σ_1 is increased gradually from a negative value, we have small amplitudes nonlinear periodic solutions for a_1 and a_2 until they reach the point A. Then they increased at a remarkable rate until reach the point B, at this point B, we have a saddle-node bifurcation. Subsequent to this bifurcation, there is a jump from large- to small amplitudes i.e. (jump from B to C). Then they move along D–I until reach the point E, at this point E, we have another saddle-node bifurcation. Subsequent to this bifurcation, there is a jump from large- to small amplitudes i.e. (jump from E to F). Then they move with small amplitudes nonlinear periodic solutions. As σ_1 is decreased gradually from a large positive value, we have small amplitudes nonlinear periodic solutions for a_1 and a_2 until they reach the point G. Then they are increased at a remarkable rate until they reach the point H, at this point H, we have a saddle-node bifurcation. Subsequent to this bifurcation, there is a jump

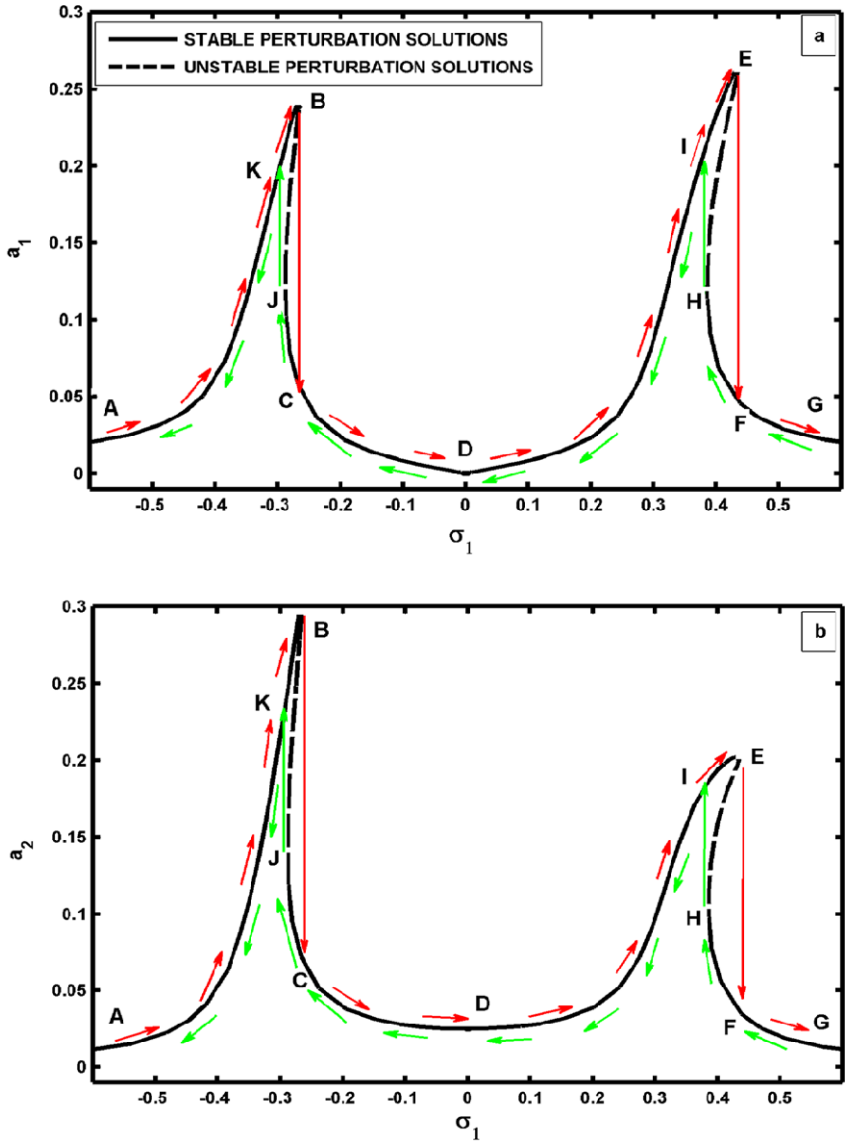

Fig. 2 Frequency-response curves of: (**a**) the main system and (**b**) the controller

from small to large amplitudes i.e. (jump from H to I). Then they move along D–C until they reach the point J, at this point J, we have another saddle-node bifurcation. Subsequent to this bifurcation, there is a jump from small to large amplitudes i.e. (jump from J to K).

The influence of the control signal gain γ on the frequency-response curves of both the main system and the controller is presented in Figs. 3a and 3b, respectively. Figure 3a shows that, for large values of γ, the vibration reduction frequency bandwidth of the controller is wider, and Fig. 3b shows that, for large values of γ, the controller amplitude decreases.

The effects of the feedback signal gain λ on the frequency-response curves of the main system and the controller is presented in Figs. 4a and 4b, respectively. Here Fig. 4a shows that, as the feedback signal gain λ increases, the vibration reduction frequency bandwidth of the controller is wider, and Fig. 4b shows that, for large values of λ, the controller peak amplitudes increases.

Based on Fig. 5, for a negative or positive values of the controller's cubic nonlinear parameter α_2, the frequency-response curve is either bent to the right (hard spring) or to the left (soft spring), respectively.

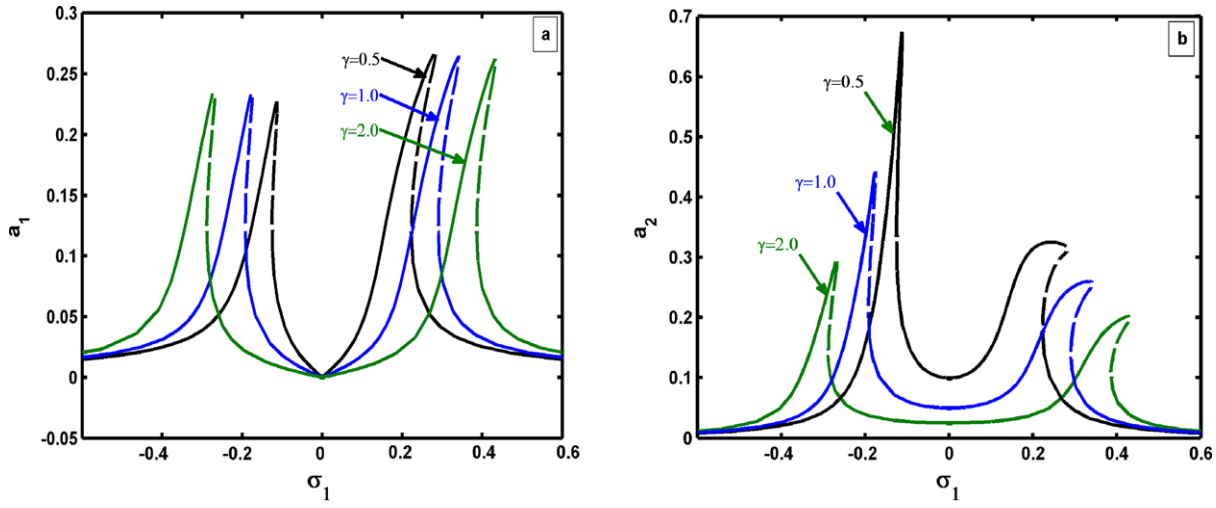

Fig. 3 Effect of varying the control signal gain γ on the frequency-response curves of: (**a**) the main system, and (**b**) the controller

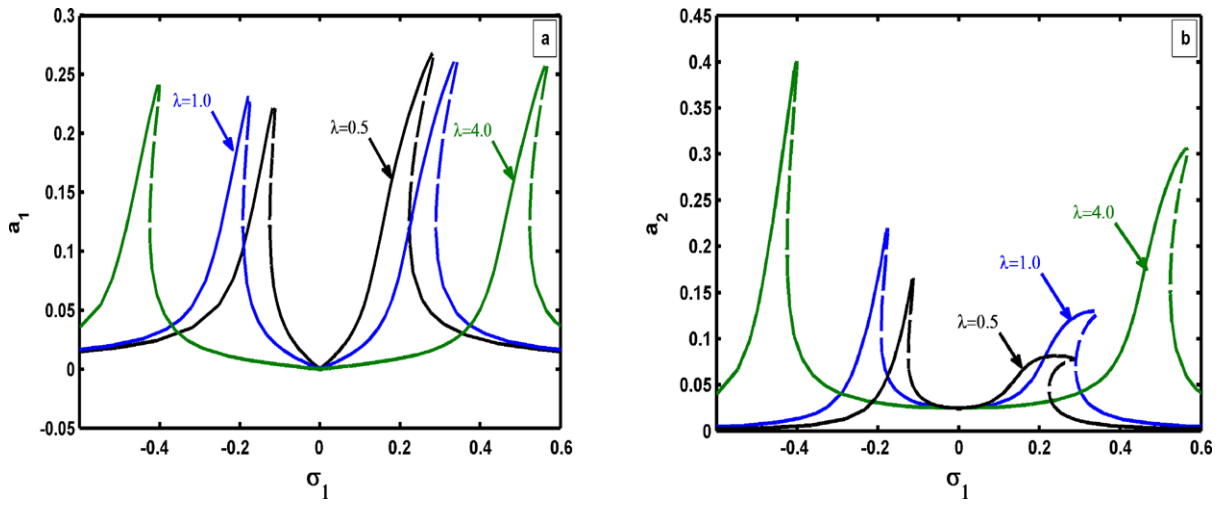

Fig. 4 Effect of varying the feedback signal gain λ on the frequency-response curves of: (**a**) the main system, and (**b**) the controller

Figure 6 shows the effect of the controller's damping coefficient μ_2 values on both the main system and the controller frequency-response curves. It is noted that the existence of multiple solution and bifurcation points depends on the damping coefficient value. Here, for small values of damping coefficient μ_2, the jumping phenomenon occurs. For large values of damping coefficient μ_2, both the main system and the controller exhibits linear responses and the jumping phenomenon disappears. It is noted that, as μ_2 increases, the controller's efficiency to eliminate the primary resonance excitations slightly decreases, but the main system and the controller peak amplitudes decreases.

Figure 7 shows the frequency response-curves of both the main system and the controller for three different values of the internal detuning parameter σ_2. Here, Fig. 7a shows that for $\sigma_2 = -0.2$ the minimum main system steady-state amplitude occurs when $\sigma_1 = -0.2$, for $\sigma_2 = 0.0$ the minimum main system steady-state amplitude occurs when $\sigma_1 = 0.0$, and for $\sigma_2 = 0.2$ the minimum main system steady-state amplitude occurs when $\sigma_1 = 0.2$. Based on Fig. 7a the minimum main system steady-state amplitude occurs when $\sigma_1 = \sigma_2$ i.e. ($\omega_2 = \Omega$ from (19)). This means that it is necessary to tune the controller's natural frequency ω_2 to the same value of the excitation fre-

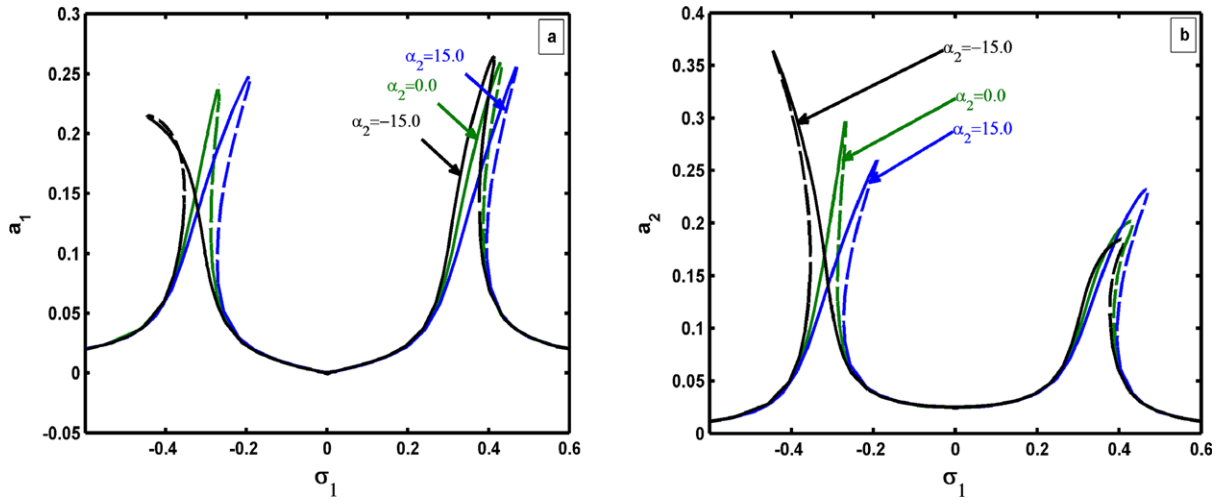

Fig. 5 Effect of varying the nonlinear parameter α_2 on the frequency-response curves of: (**a**) the main system, and (**b**) the controller

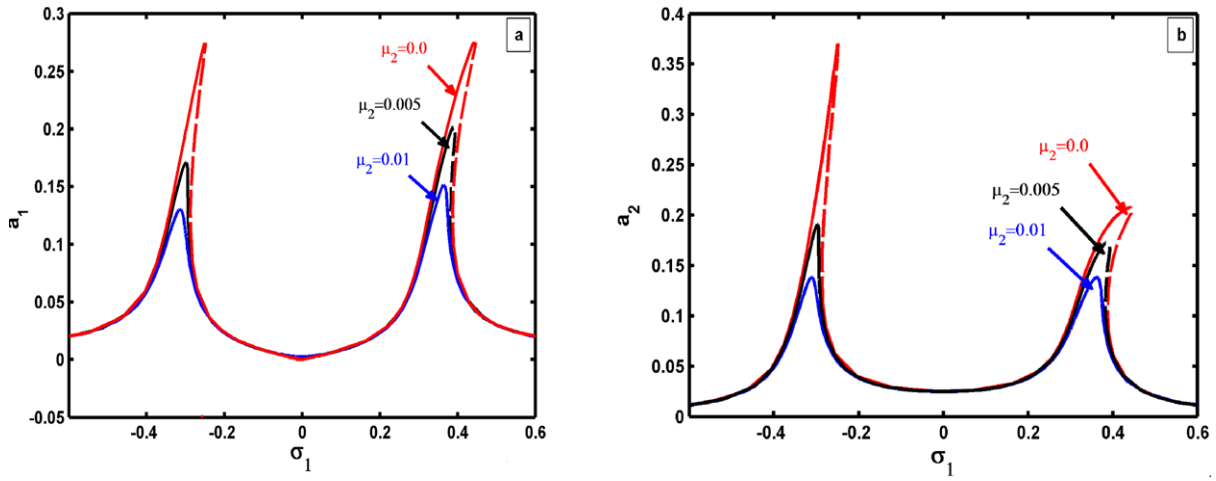

Fig. 6 Effect of varying the controller damping coefficient μ_2 on the frequency-response curves of: (**a**) the main system, and (**b**) the controller

quency Ω rather than the main system's natural frequency ω_1. So, for the dynamical systems subject to a variable external excitation frequency Ω, we can measure the variation in the excitation frequency Ω then, the controller natural frequency ω_2 is modified adaptively to the same new value of the excitation frequency. All these results were verified numerically in Sect. 7.

Based on the linear control theory, the dynamical systems static gains are inversely proportional to the square of the natural frequency. So, the small natural frequency systems have a large static gain, which is an undesirable phenomenon in vibration control theory. Figure 8 shows the effects of decreasing the natural frequency of both the main system and the controller on their frequency-response curves for internal detuning parameter $\sigma_2 = 0$ i.e. $(\omega_1 = \omega_2)$. The figure shows that, as ω_1 and ω_2 decrease, the peak amplitudes of both the main system and the controller increase, and the vibration reduction controller frequency bandwidth increases. So this type of controllers (PPF) is very suitable for small natural frequency dynamical systems that subjected to primary resonance excitations.

Figure 9 shows the frequency-response curves of the closed-loop case for various levels of the excita-

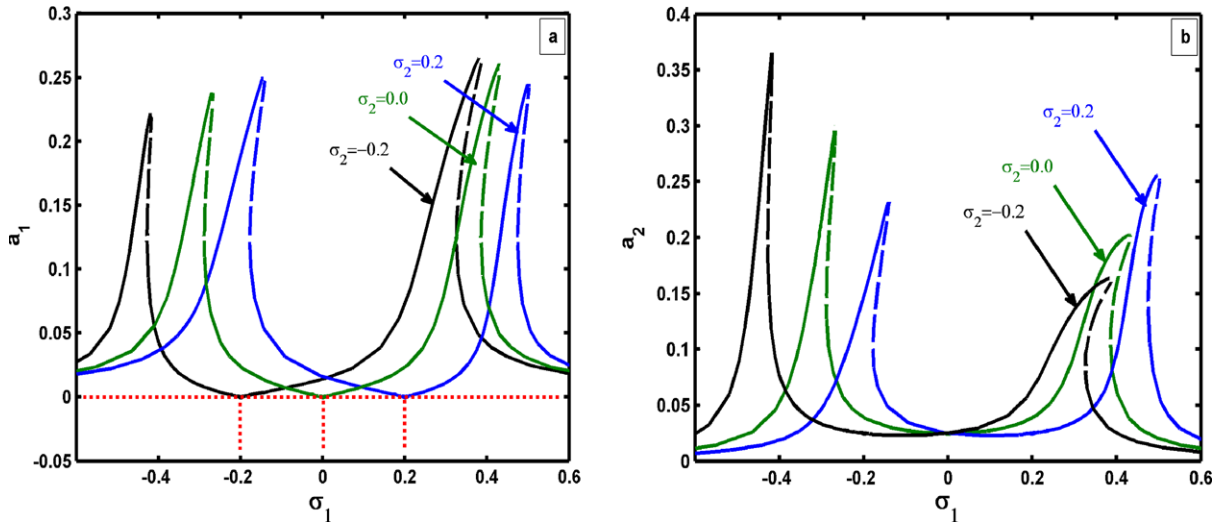

Fig. 7 Effect of varying the internal detuning parameter σ_2 on the frequency-response curves of: (**a**) the main system, and (**b**) the controller

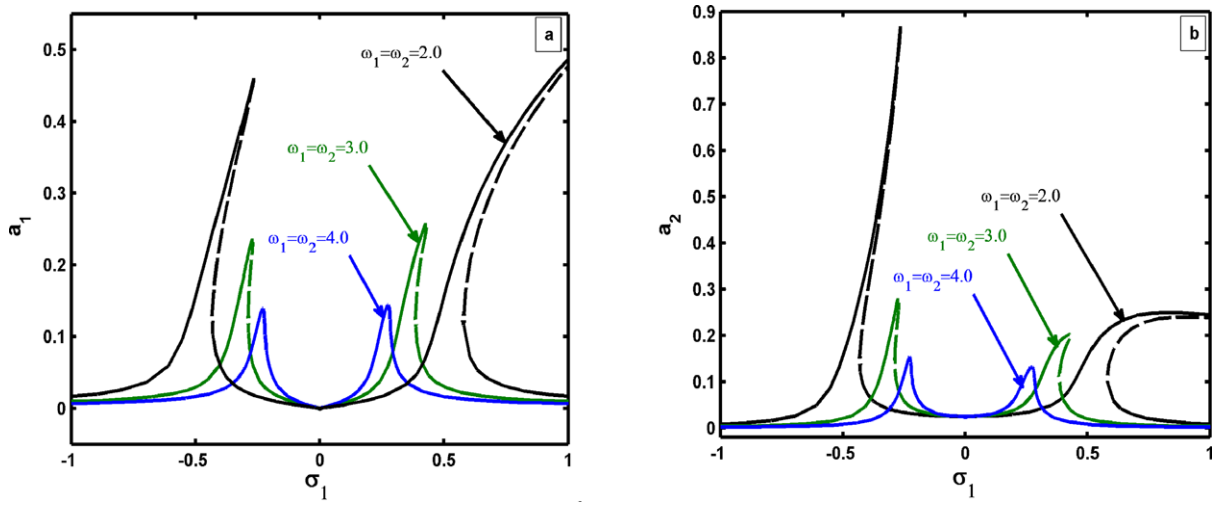

Fig. 8 Effect of varying the natural frequency for $\sigma_2 = 0$ (i.e. $\omega_1 = \omega_2$) on the frequency-response curves of: (**a**) the main system, and (**b**) the controller

tion amplitude f. It is clear that, as the excitation amplitude increases, the frequency-response curves bend away from the linear curves, resulting in multivalued regions and jump phenomenon. The figure shows that the minimum steady-state amplitude of the main system occurs for the detuning parameters $\sigma_1 = \sigma_2 = 0$.

In Fig. 10, we show typical force-response curves of both the main system and the controller for four different values of the external detuning parameter σ_1 at the presence of 1:1 internal resonance (i.e. $\sigma_2 = 0.0$). We can trace the histories of a_1 and a_2 as the excitation amplitude f slowly increased from zero. Initially both a_1 and a_2 are zeros, and they follow the curve according to the external detuning parameter σ_1 values. For $\sigma_1 = 0$, the main system steady-state amplitude a_1 increases slightly, while the controller steady-state amplitude a_2 increases rapidly in a linear form as the excitation amplitude f increases. For $\sigma_1 \neq \sigma_2$, the main system steady-state amplitude a_1 increases rapidly as with the controller steady-state amplitude a_2; and we can note possible jump phenomena and unstable behaviors occurrence. This confirms the failure of the

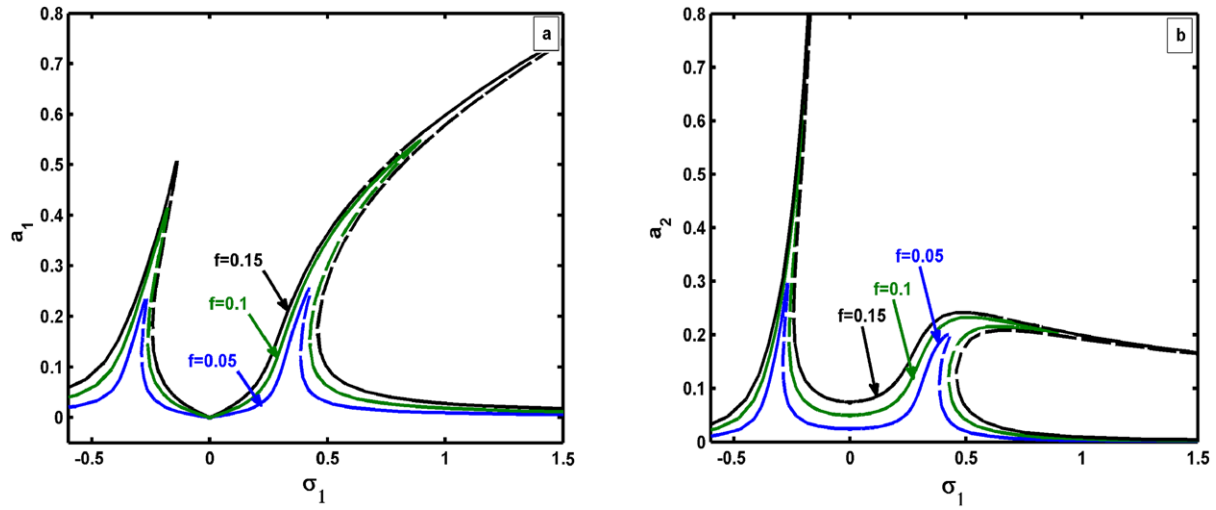

Fig. 9 Effect of varying the excitation force f on the frequency-response curves of: (**a**) the main system, and (**b**) the controller

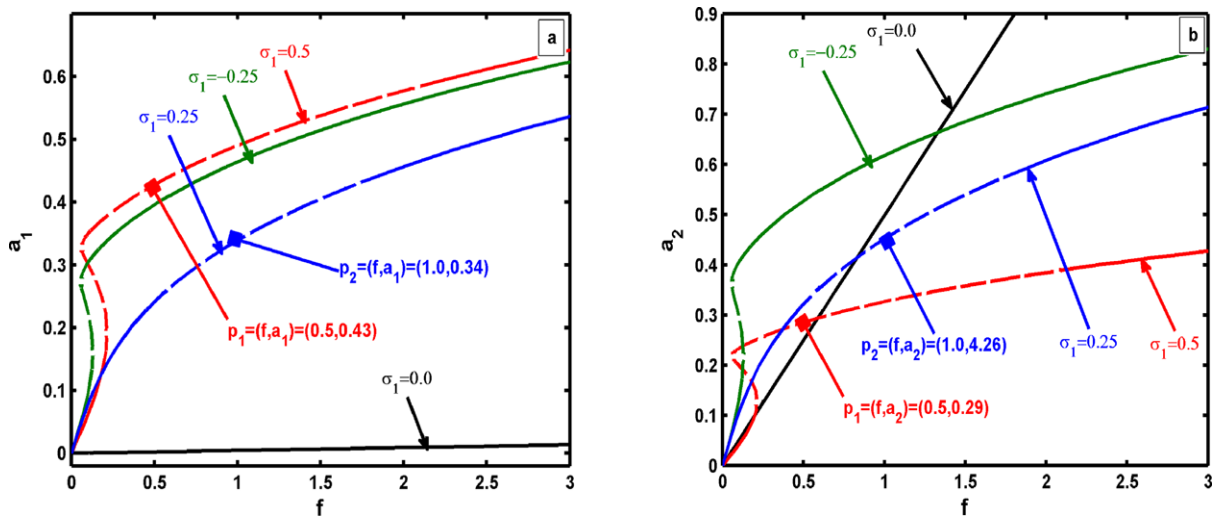

Fig. 10 Force-amplitude response curves when $\sigma_2 = 0$ of: (**a**) the main system, and (**b**) the controller

PPF controller to suppress the primary resonance vibrations for small external detuning, if it retains the status of the internal resonance.

The variations of σ_2 versus a_1 and a_2 are plotted in Fig. 11 in the case of primary resonance excitations (i.e. $\sigma_1 = 0.0$). Based on Fig. 11, the main system exhibits minimum stable steady-state amplitude when $\sigma_2 = 0.0$. For $\sigma_2 \leq -3$ this means that $\omega_2 \leq 0$, which cannot occur from the engineering point of view, the frequency-response curves for both the main system and controller exhibit unstable response. The figure shows also for mistuning between ω_1 and ω_2 it is preferable for the system that ω_2 must be smaller than ω_1.

7 Numerical simulations

To validate the results of multiple scales perturbation analysis, the analytical results were verified by integration of the original equations (3) and (4) numerically, and the numerical results for steady-state solutions are marked as small circles on Figs. 12, 13, 14, 15. In Fig. 12, a_1 and a_2 are plotted versus σ_1 for

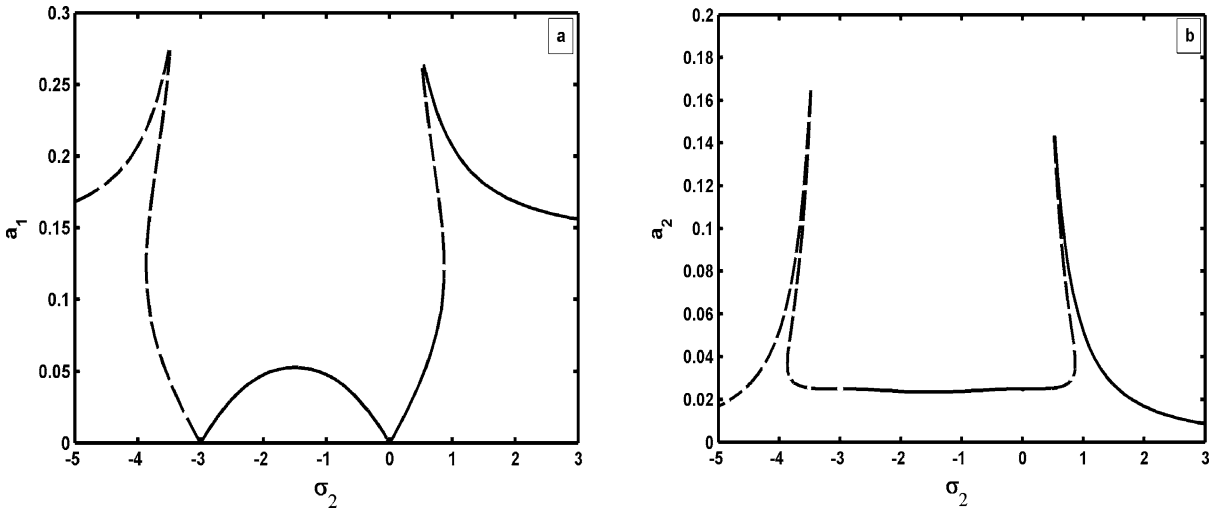

Fig. 11 Effect of varying the internal detuning parameter σ_2 on the frequency-response curves of: (**a**) the main system, and (**b**) the controller

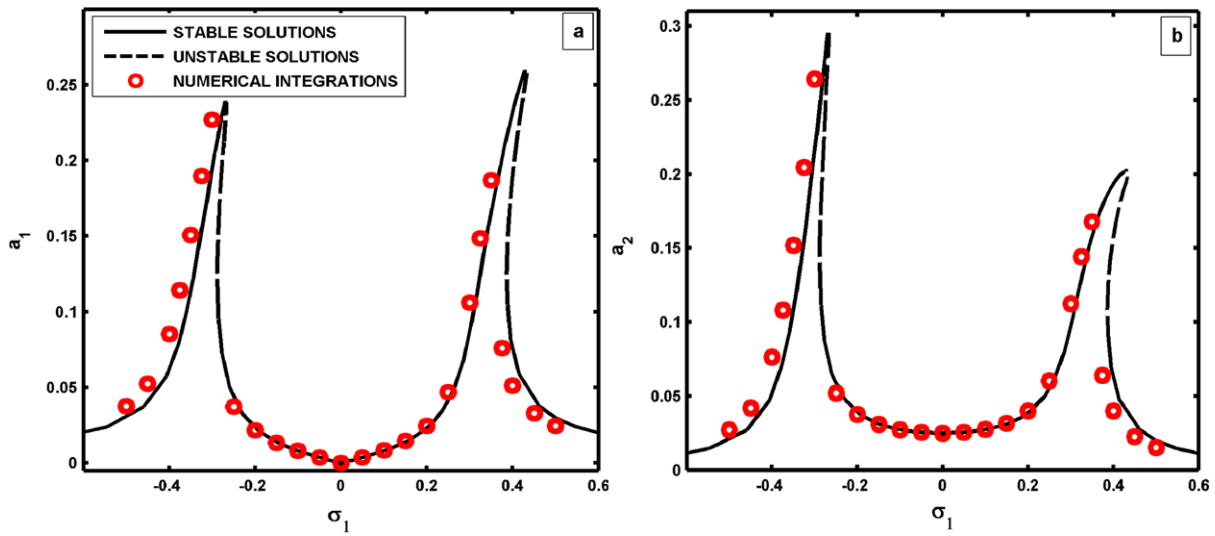

Fig. 12 The frequency-response curves for $\mu_2 = 0.001$ of: (**a**) the main system and (**b**) the controller

$\mu_2 = 0.001$. In this case jump phenomena were reported for a_1 and a_2. In Fig. 13, a_1 and a_2 are plotted versus σ_1 for $\mu_2 = 0.01$, in this case no jump phenomenon was observed. In Fig. 14, a_1 and a_2 are plotted as a functions in f for $\sigma_1 = \sigma_2 = 0$. In Fig. 15, a_1 and a_2 are plotted as a function of f for $\sigma_1 = 0.25$ and $\sigma_2 = 0.0$. Based on Figs. 12, 13, 14, 15 the analyses show that all predictions from the analytical solutions are in good agreement with the numerical simulation.

Figures 16 and 17 show the time responses for zero initial conditions of the main system for the open and the closed loop cases, respectively, for the system parameters mentioned in Sect. 6. It can be seen from the figures that the main system's steady-state amplitude in the control case was reduced by about **98.5** % from its value without control. This means that the effectiveness of the PPF controller E_a is about **625** (E_a = steady-state amplitude of the main system without controller/steady-state amplitude of the main system with controller).

Based on Fig. 7, Figs. 18, 19, 20, 21, 22 show the time responses for zero initial conditions of the main

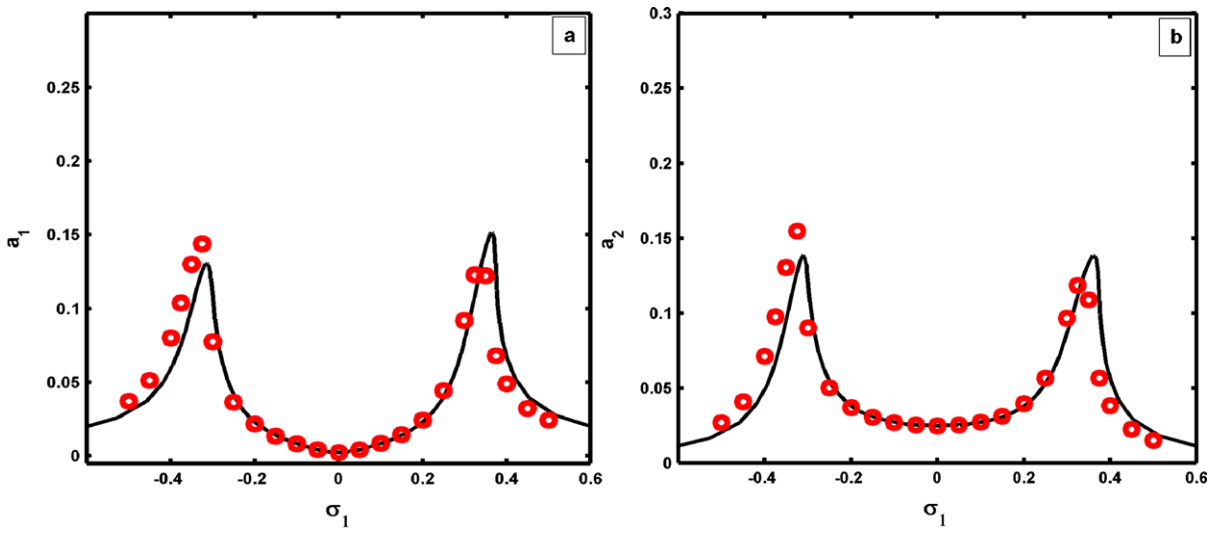

Fig. 13 The frequency-response curves for $\mu_2 = 0.01$ of: (**a**) the main system, and (b) the controller

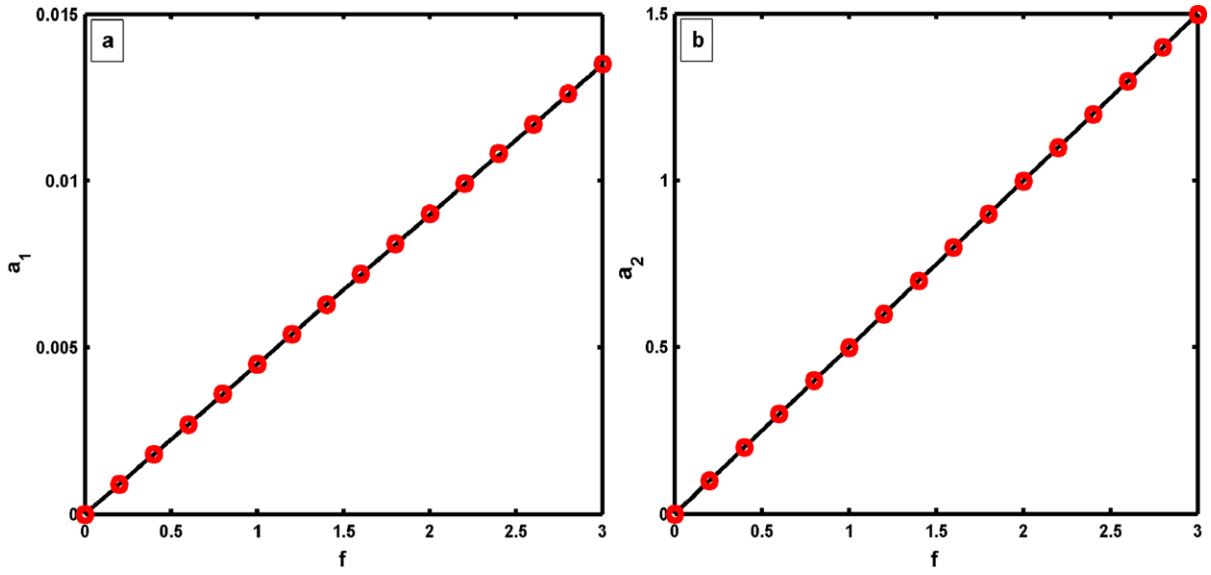

Fig. 14 Force-amplitude response curves for $\sigma_1 = \sigma_2$ i.e. ($\Omega = \omega_2$) of: (**a**) the main system and (**b**) the controller

system and the controller for different values of the detuning parameters σ_1, σ_2, and the excitation force f.

Figures 18 and 19 show the main system and the controller time response for $f = 0.05$ and $f = 3.0$, respectively, where $\sigma_1 = \sigma_2 = 0.0$. The figures show that the main system steady-state amplitudes reached to a very small value. Figures 19 shows that the main system time response may take more time until it reaches the steady-state because of the high excitation force.

Figures 20 and 21 show the main system and the controller time response for $\sigma_1 = \sigma_2 = 0.25$ and $\sigma_1 = \sigma_2 = 0.5$, respectively, where $f = 0.5$. The figures show that the main system steady-state amplitudes reached to a very small value. Figure 21 shows that the main system may take more time until it reaches the steady-state because of the large detuning values.

Figure 22 shows the main system and the controller time response for $f = 0.5, \sigma_1 = 0.25$ and $\sigma_2 = 0.0$. The figure shows that the main system steady-state

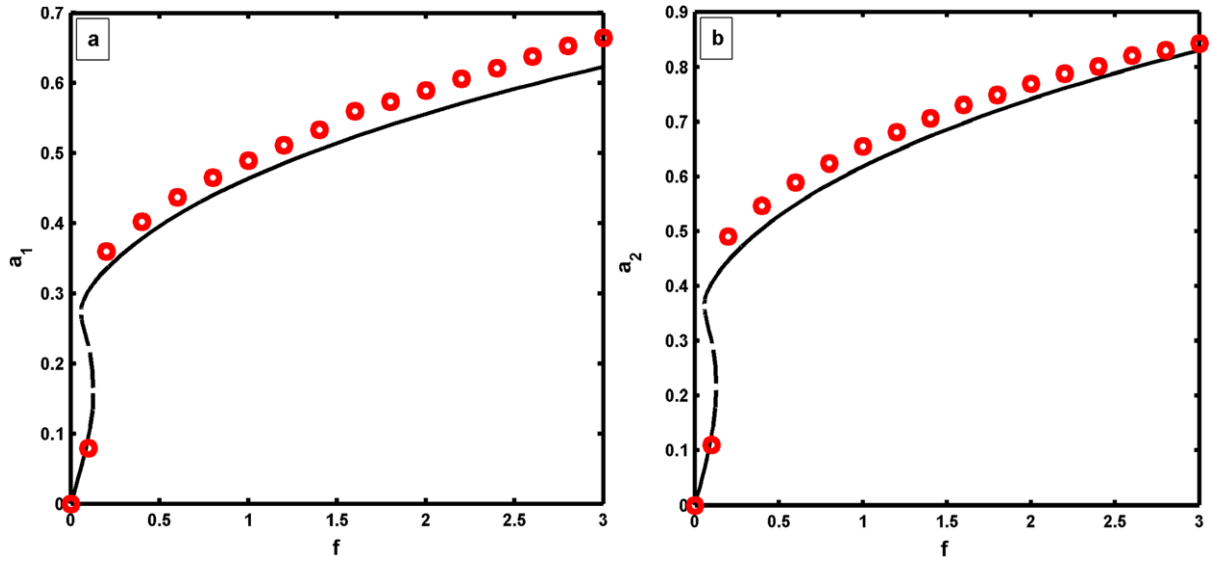

Fig. 15 Force-amplitude response curves for $\sigma_1 = 0.25, \sigma_2 = 0$ of: (**a**) the main system, and (**b**) the controller

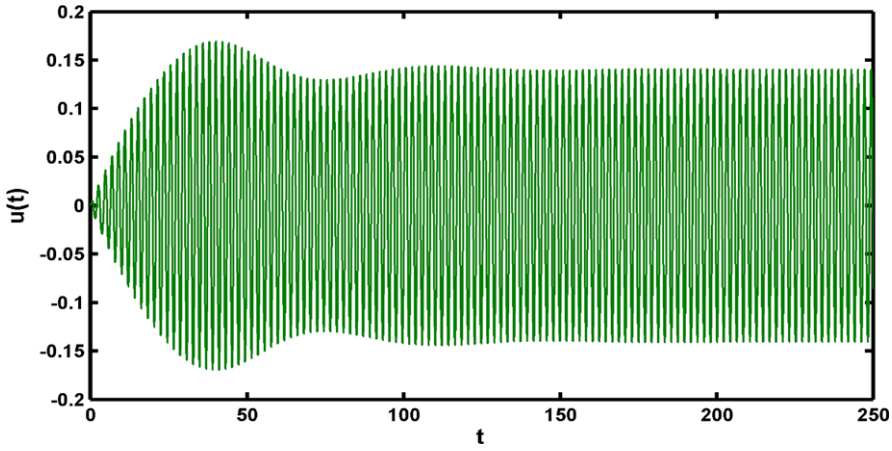

Fig. 16 The main system time response of the open loop case for $\Omega = \omega_1 = 3.0, \sigma_1 = 0$ and $f = 0.05$

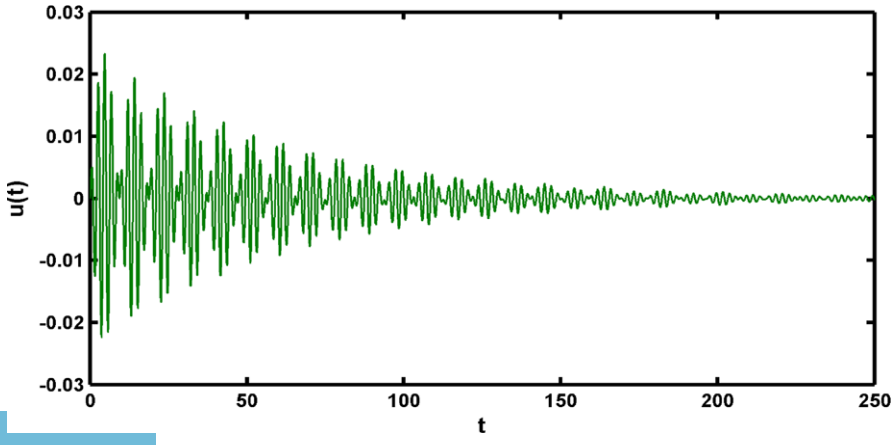

Fig. 17 The main system time response of the closed loop case for $\omega_1 = \omega_2 = \Omega = 3.0, \sigma_{1,2} = 0$ and $f = 0.05$

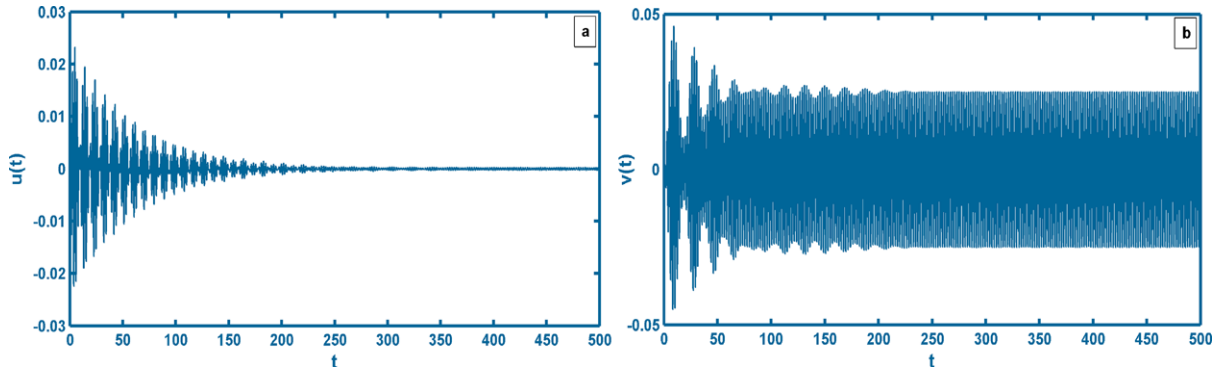

Fig. 18 Time responses for $\sigma_1 = \sigma_2 = 0.0, \omega_1 = 3.0, f = 0.05$ of: (**a**) the main system, (**b**) the controller

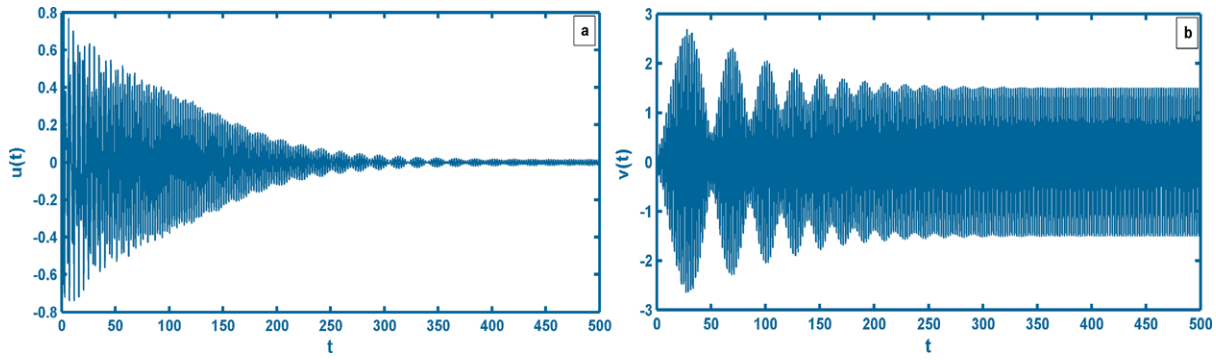

Fig. 19 Time responses for $\sigma_1 = \sigma_2 = 0.0, \omega_1 = 3.0, f = 3.0$ of: (**a**) the main system, and (**b**) the controller

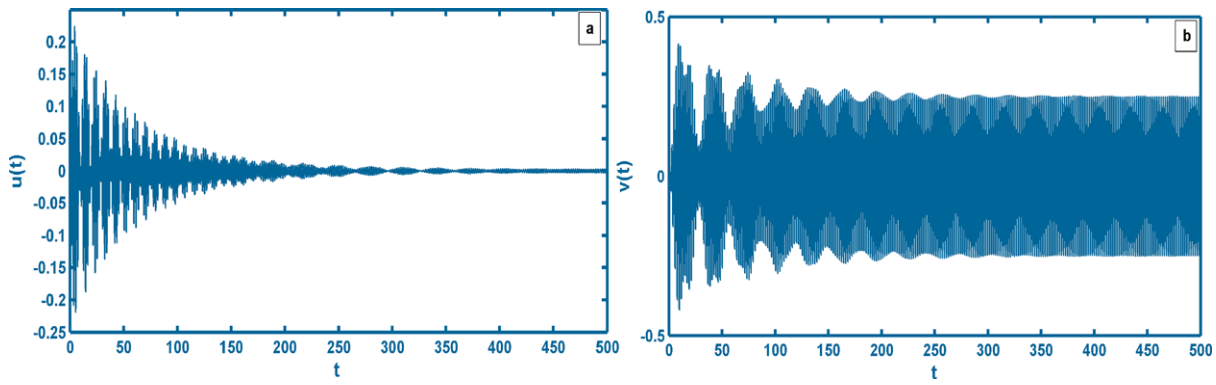

Fig. 20 Time responses for $\sigma_1 = \sigma_2 = 0.25, \omega_1 = 3.0, f = 0.5$ of: (**a**) the main system, and (**b**) the controller

amplitudes reached a large significantly value because of $\sigma_1 \neq \sigma_2$.

Based on Figs. 18, 19, 20, 21, 22 the controller operates effectively to eliminate the main system vibration amplitude when $\sigma_1 = \sigma_2$ i.e. ($\Omega = \omega_2$). Under this condition, all excess energy in the excited system is channeled to the controller.

According to the unstable points P_1 and P_2 that are marked on Fig. 10, the main system and the controller time response were examined. As shown in Figs. 23a, 23b (according to the point P_1) and Figs. 24a, 24b (according to the point P_2), the main system and the controller time response exhibit unstable motions. So, we construct Poincaré maps for each response to deter-

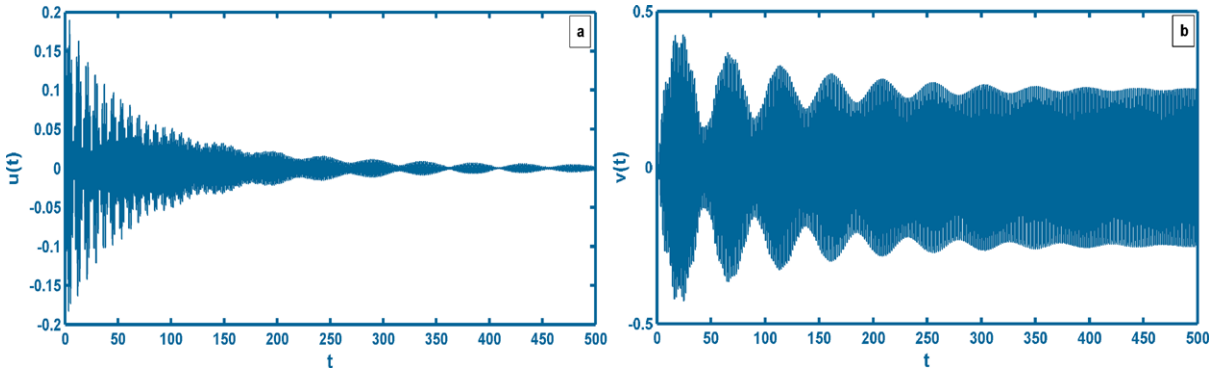

Fig. 21 Time responses for $\sigma_1 = \sigma_2 == 0.5, \omega_1 = 3.0, f = 0.5$ of: (**a**) the main system, and (**b**) the controller

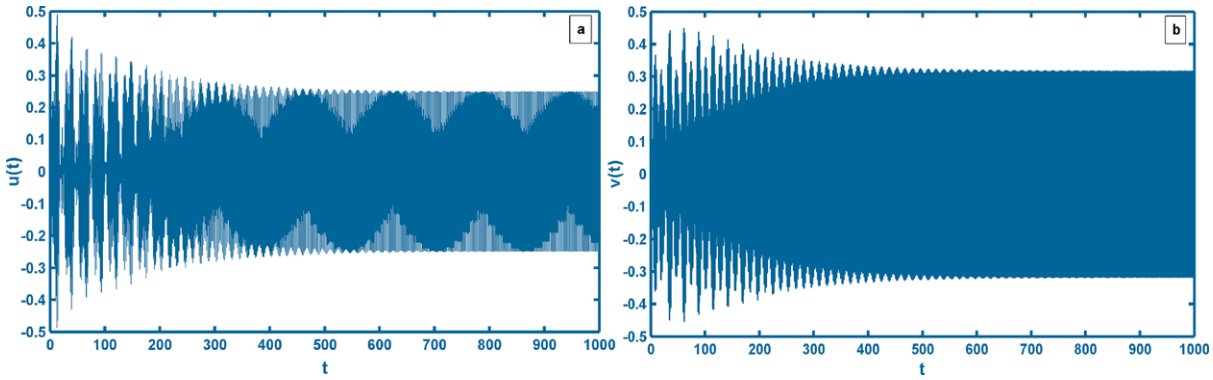

Fig. 22 Time responses for $\sigma_1 = 0.25, \sigma_2 = 0.0, \omega_1 = 3.0, f = 0.5$ of: (**a**) the main system, and (**b**) the controller

mine the nature of these motions as shown in Figs. 23c, 23d (according to the point P_1) and Figs. 24c, 24d (according to the point P_2), which shows a quasi-periodic motion for both the main system and the controller.

8 Comparison between time response solutions of the perturbation and the numerical methods

The set of (34a)–(34d) describes modulation of the amplitudes a_1, a_2 and the modified phases φ_1, φ_2 for the tested case of two resonances occurring simultaneously ($\Omega = \omega_1, \omega_1 = \omega_2$). The numerical solutions of (34a)–(34d) for chosen values of the system parameters are presented graphically in Figs. 25 and 26. The dashed lines show the modulation of the amplitudes for the generalized coordinates u and v. However, the continuous lines represent the time history of vibrations which were obtained numerically as solutions of the original equations (3) and (4). The solutions presented in the graphs were obtained by adopting the same values of the system parameters as mentioned in Sect. 6, except the excitation amplitude f and the external detuning parameter σ_1. Here, for Fig. 25 $f = 3.0$ and $\sigma_1 = 0.0$, and for Fig. 26 $f = 0.5$ and $\sigma_1 = 0.25$. The simulation results show that (34a)–(34d) describe with great precision not only the steady-state modulating amplitudes but also the transient modulating amplitudes of the original equations solutions.

9 Conclusions

The positive position feedback (PPF) controller has been studied for the primary resonance of a nonlinear system in the presence of 1:1 internal resonance. The method of multiple scales is used to derive four first order differential equations governing the time evolution of the amplitudes and phases of both the main system and the controller. Then, the bifurcation analysis is conducted to examine the stability of the closed loop

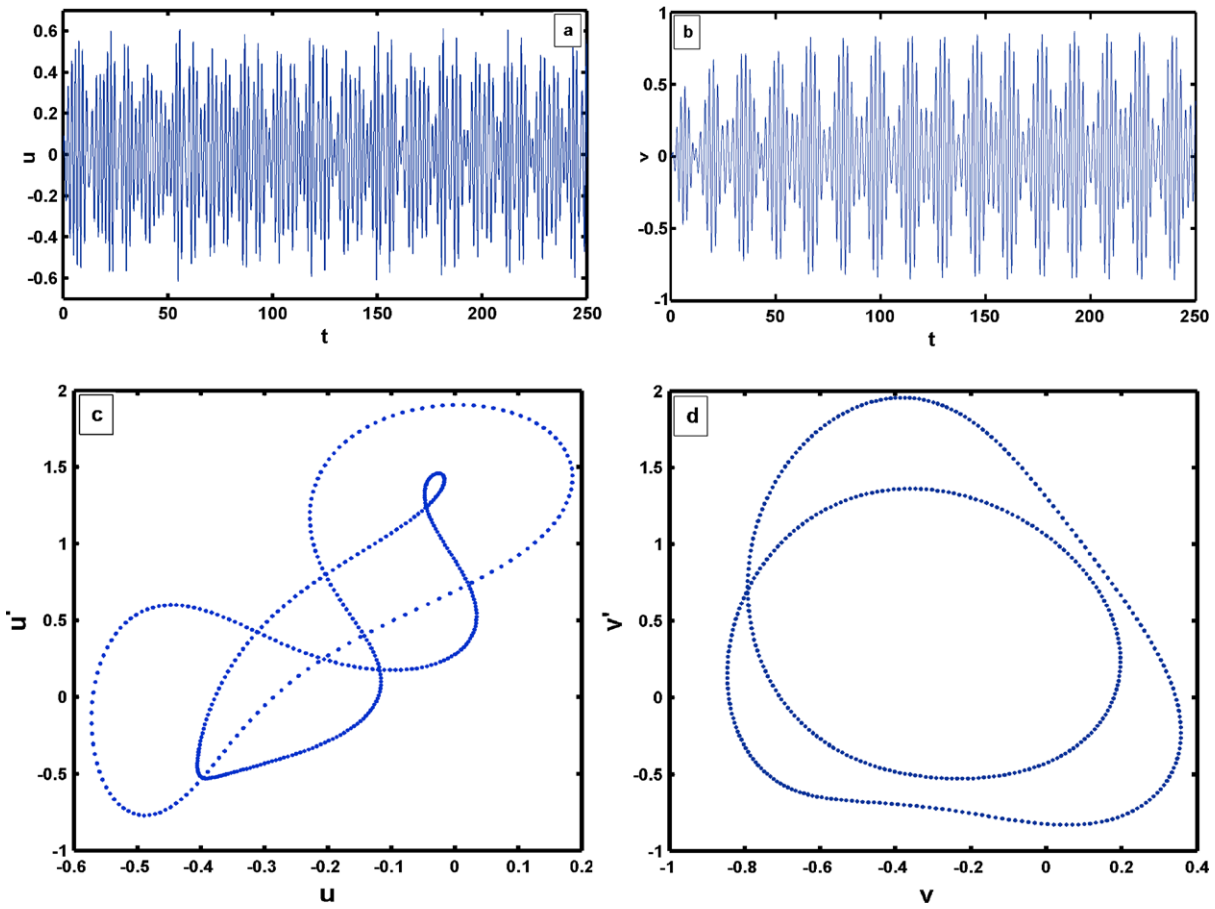

Fig. 23 (**a**, **b**) Time responses of the main system and the controller, respectively; (**c**, **d**) Poincaré maps of the main system and the controller, respectively; for $\sigma_1 = 0.25, \sigma_2 = 0.0, \omega_1 = 3.0, f = 1.0$

case and to investigate the performance of the control law. The analysis revealed that:

1 Once the controller natural frequency is properly tuned to the excitation frequency ($\Omega = \omega_2$), the PPF controller is very effective in reducing the high amplitude vibration of the nonlinear systems.
2 This type of controller (PPF) is very suitable for vibration reduction of small natural frequencies dynamical systems.
3 The effective frequency bandwidth of the controller can be controlled via the control signal gain γ, and the feedback signal gain λ values. The effective frequency bandwidth of the controller may shrink or widen as γ and λ decreases or increases, respectively, as shown in Figs. 3 and 4.
4 Decreasing the controller damping coefficient μ_2, increasing the controller efficiency for vibration suppression. The best performance is obtained when $\mu_2 = 0.0$ as reported in Ref. [21].
5 In order that the controller is operating in the best condition $\sigma_1 \approx \sigma_2$, it is possible to measure the variation in the excitation frequency Ω; then the controller natural frequency ω_2 is modified adaptively to the same new value of the excitation frequency.

10 Comparison with previously published work

In comparison with previous work [1], the authors studied numerically and experimentally four types of controllers that applied to nonlinear beam model. The result for a single beam system shows that PPF controller and nonlinear saturation controller (NSC) are the most effective ones for the assumed conditions of the considered system but an analytical study for the

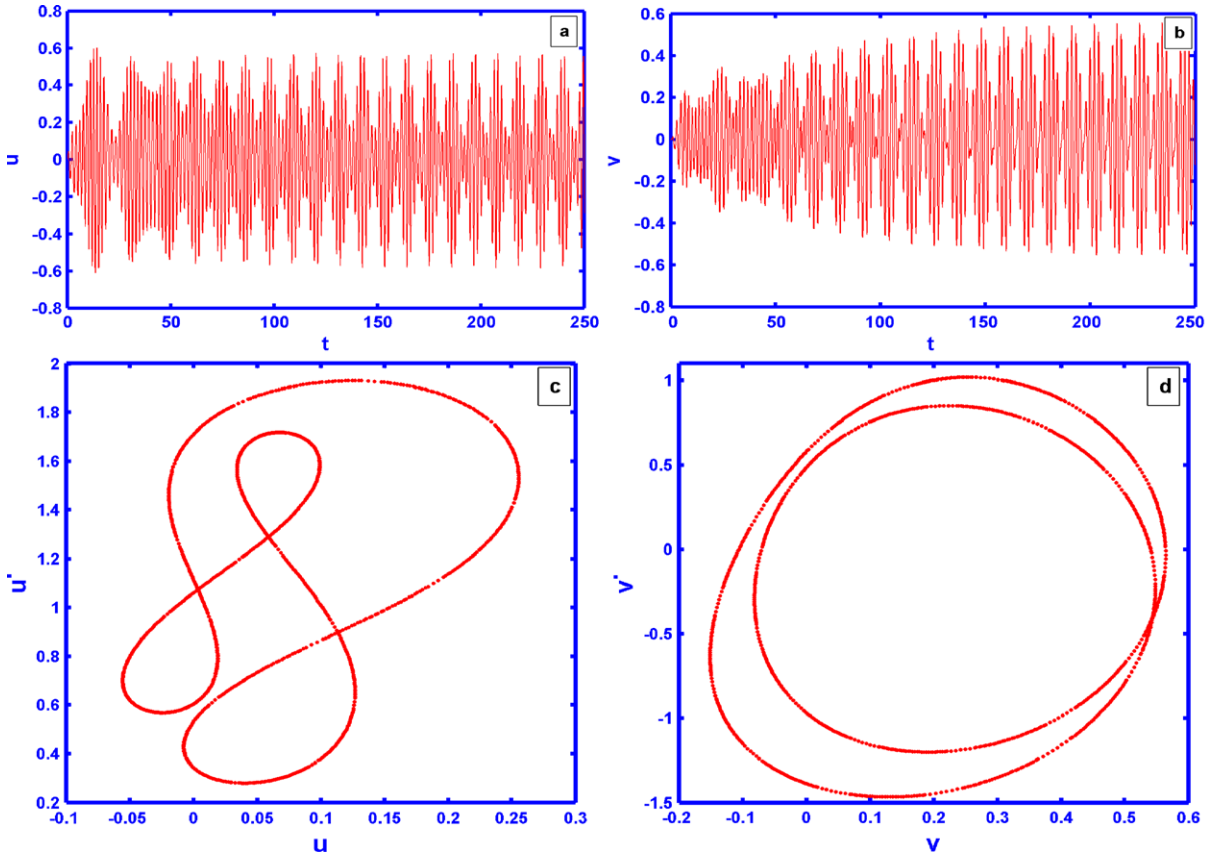

Fig. 24 (**a**, **b**) Time responses of the main system and the controller, respectively; (**c**, **d**) Poincaré maps of the main system and the controller, respectively; for $\sigma_1 = 0.5, \sigma_2 = 0.0, \omega_3 = 3.0, f = 0.5$

NSC system only has been presented. Positive position feedback (PPF) controller applied for a flexible manipulator is presented by Shan et al. [2]. The authors considered several vibration modes in the control strategy for a linear mathematical model of the system. The PPF was compared with the algorithm of velocity feedback. Experimental investigation showed that only the PPF algorithm is able to work properly while the slewing process is realized. In Ref. [3], two control algorithms, the state feedback pole assignment and the positive position feedback, were implemented to control the first-order mode of the system vibration actively. The experimental results showed that the positive position feedback is the better both in the control speed and in the attenuation amplitude than the state feedback pole assignment.

In this paper, an analytical study for positive position feedback controller that coupled to a nonlinear system was presented. The effect of all controller parameters was investigated. The steady-state solutions and its stability were presented. We found that, for the effective PPF controller, it is necessary tuning the controller natural frequency to the external excitation frequency ($\Omega = \omega_2$) as shown in Fig. 7. In the case of ($\Omega = \omega_2$) the relation between the modal amplitudes a_1, a_2 and the excitation force f is linear for a wide range of the excitation force.

We found that all predictions from analytical solutions are in good agreement with the numerical simulation.

Appendix

$$r_{11} = -\mu_1\omega_1$$

$$r_{12} = \frac{1}{2\omega_1} f\cos(\varphi_{10})$$

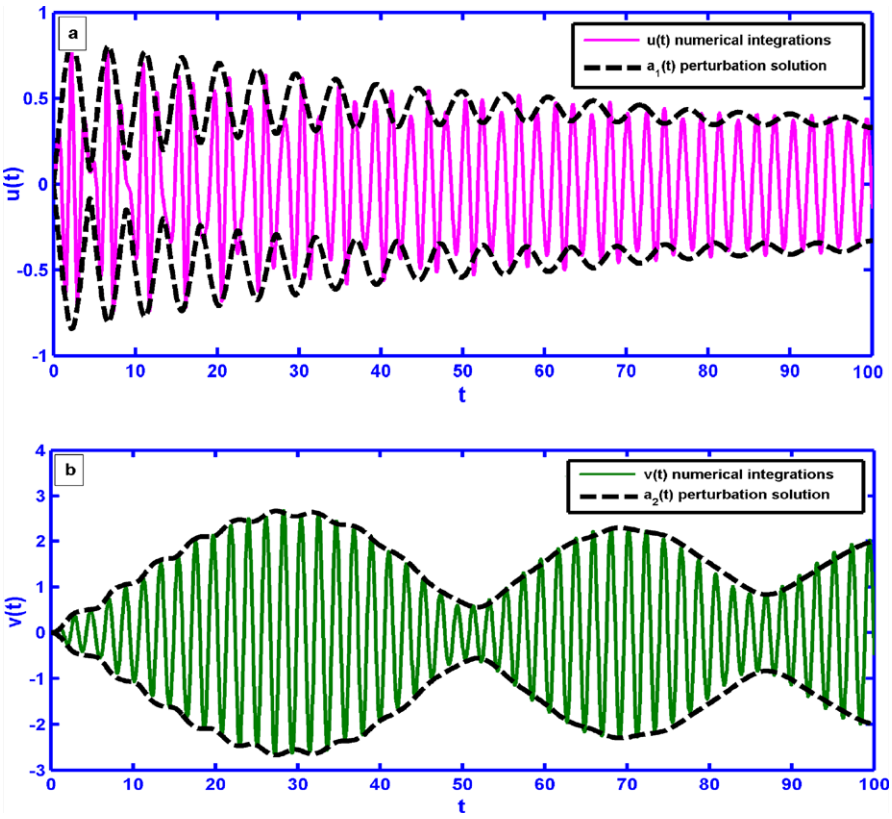

Fig. 25 Time responses for $\sigma_1 = \sigma_2 = 0.0, \omega_1 = 3.0, f = 3.0$ of: (**a**) the main system, (**b**) the controller

$$r_{13} = \frac{1}{2\omega_1}\gamma \sin(\varphi_{20})$$

$$r_{14} = \frac{1}{2\omega_1}\gamma a_{20} \cos(\varphi_{20})$$

$$r_{21} = -\frac{3}{4\omega_1}\alpha_1 a_{10} - \frac{1}{2}\delta\omega_1 a_{10} - \frac{1}{2\omega_1 a_{10}^2}\gamma a_{20}\cos(\varphi_{20}) - \frac{1}{2\omega_1 a_{10}^2} f \cos(\varphi_{10})$$

$$r_{22} = -\frac{1}{2\omega_1 a_{10}} f \sin(\varphi_{10})$$

$$r_{23} = \frac{1}{2\omega_1 a_{10}}\gamma \cos(\varphi_{20})$$

$$r_{24} = -\frac{1}{2\omega_1 a_{10}}\gamma a_{20} \sin(\varphi_{20})$$

$$r_{31} = -\frac{1}{2\omega_2}\lambda \sin(\varphi_{20})$$

$$r_{32} = 0$$

$$r_{33} = -\mu_2\omega_2$$

$$r_{34} = -\frac{1}{2\omega_2}\lambda a_{10}\cos(\varphi_{20})$$

$$r_{41} = -\frac{1}{2}\delta\omega_1 a_{10} - \frac{3}{4\omega_1}\alpha_1 a_{10} - \frac{1}{2\omega_1 a_{10}^2}\gamma a_{20}\cos(\varphi_{20}) - \frac{1}{2\omega_2 a_{20}}\lambda\cos(\varphi_{20}) - \frac{1}{2\omega_1 a_{10}^2} f\cos(\varphi_{10})$$

$$r_{42} = -\frac{1}{2\omega_1 a_{10}} f \sin(\varphi_{10})$$

$$r_{43} = \frac{3}{4\omega_2}\alpha_2 a_{20} + \frac{1}{2\omega_1 a_{10}}\gamma\cos(\varphi_{20}) + \frac{1}{2\omega_2 a_{20}^2}\lambda a_{10}\cos(\varphi_{20})$$

$$r_{44} = -\frac{1}{2\omega_1 a_{10}}\gamma a_{20}\sin(\varphi_{20}) + \frac{1}{2\omega_2 a_{20}}\lambda a_{10}\sin(\varphi_{20})$$

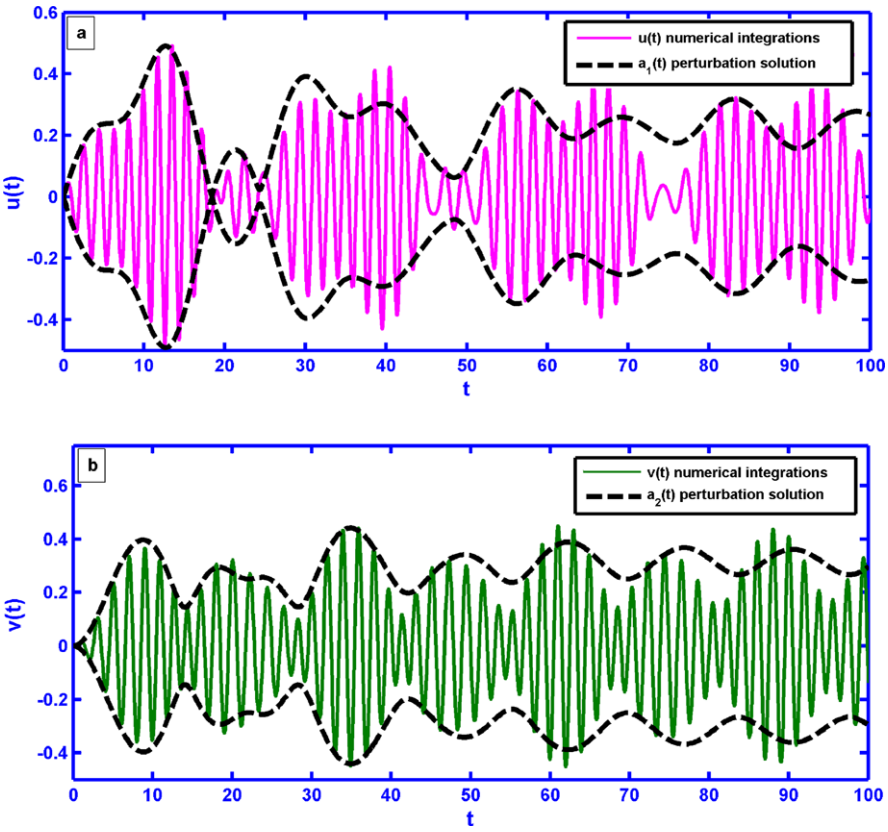

Fig. 26 Time responses for $\sigma_1 = 0.25$, $\sigma_2 = 0.0$, $\omega_1 = 3.0$, $f = 0.5$ of: (**a**) the main system, and (**b**) controller

References

1. Warminski, J., Bochenski, M., Jarzyna, W., Filipek, P., Augustyinak, M.: Active suppression of nonlinear composite beam vibrations by selected control algorithms. Commun. Nonlinear Sci. Numer. Simul. **16**, 2237–2248 (2011)
2. Shan, J., Liu, H., Sun, D.: Slewing and vibration control of a single-link flexible manipulator by positive position feedback (PPF). Mechatronics **15**, 487–503 (2005)
3. Wang, K., Xiong, S., Zhang, J.: Active vibration control of a flexible cantilever beam using piezoelectric actuators. Energy Procedia **13**, 4367–4374 (2011)
4. Creasy, M.A., Leo, D.J., Farinholt, K.M.: Adaptive positive position feedback for actively absorbing energy in acoustic cavities. J. Sound Vib. **311**, 461–472 (2008)
5. Ahamed, B., Pota, H.R.: Dynamic compensation for control of a rotary wing UAV using positive position feedback. J. Intell. Robot. Syst. **61**, 43–56 (2011)
6. Baz, A., Poh, S.: Short communications optimal vibration control with modal positive position feedback. Optim. Control Appl. Methods **17**, 141–149 (1996)
7. Baz, A., Hong, J.: Adaptive control of flexible structures using modal positive position feedback. Int. J. Adapt. Control Signal Process. **11**, 231–253 (1997)
8. El-Bassiouny, A.F.: Single-mode control and chaos of cantilever beam under primary and principal parametric excitations. Chaos Solitons Fractals **30**, 1098–1121 (2006)
9. Oueini, S.S., Nayfeh, A.H.: Single-mode control of a cantilever beam under principal parametric excitation. J. Sound Vib. **224**(1), 33–47 (1999)
10. El-serafi, S.A., Eissa, M.H., El-Sherbiny, H.M., El-Ghareeb, T.H.: Comparison between passive and active control of a non-linear dynamical system. Jpn. J. Ind. Appl. Math. **23**, 139–161 (2006)
11. Maccari, A.: Vibration control for the primary resonance of cantilever beam by a time delay state feedback. J. Sound Vib. **257**(2), 241–251 (2003)
12. Alhazza, K.A., Daqaq, M.F., Nayfeh, A.H., Inman, D.J.: Non-linear vibrations of parametrically excited cantilever beams subjected to non-linear delayed-feedback control. Int. J. Non-Linear Mech. **43**, 801–812 (2008)
13. Eissa, M., Sayed, M.: Vibration reduction of a three DOF non-linear spring pendulum. Commun. Nonlinear Sci. Numer. Simul. **13**, 465–488 (2008)
14. Eissa, M., Kamel, M., El-Sayed, A.T.: Vibration reduction of multi-parametric excited spring pendulum via transverse tuned absorber. Nonlinear Dyn. **61**, 109–121 (2010)
15. Eissa, M., Kamel, M., El-Sayed, A.T.: Vibration reduction of a nonlinear spring pendulum under multi external and parametric excitations via a longitudinal absorber. Meccanica **46**, 325–340 (2011)
16. Eissa, M., Kamel, M., El-Sayed, A.T.: Vibration suppression of a four-degree-of-freedom nonlinear spring pendulum via a longitudinal and transverse absorber. J. Appl. Mech. **79**(1), 011007 (2012)

17. Eissa, M., EL-Ganaini, W.A.A., Hamed, Y.S.: Saturation, stability and resonance of non-linear systems. Physica A **356**, 341–358 (2005)
18. Eissa, M.: Vibration and chaos control in I.C engines subjected to harmonic torque via non-linear absorbers. In: Second International Symposium on Mechanical Vibrations (ISMV-2000), Islamabad, Pakistan (2000)
19. Eissa, M., El-Ganaini, W.A.A.: Multi absorbers for vibration control of non-linear structures to harmonic excitations. Part I. In: ISMV Conference. Islamabad, Pakistan (2000)
20. Eissa, M., El-Ganaini, W.A.A.: Multi absorbers for vibration control of non-linear structures to harmonic excitations. Part II. In: ISMV Conference. Islamabad, Pakistan (2000)
21. Eissa, M.: Vibration control of non-linear mechanical system via a neutralizer. Electronic Bulletin, No. 16, Faculty of Electronic Engineering, Menouf, Egypt, 1999, July
22. Nayfeh, A., Mook, D.: Nonlinear Oscillations. Wiley, New York (1995)